

PAPILLARY MUSCLES ANALYSIS FROM HIGH RESOLUTION CT USING SPATIAL-TEMPORAL SKELETON EXTRACTION

Lin Zhong¹, Shaoting Zhang¹, Mingchen Gao¹, Junzhou Huang²,
Zhen Qian³, Dimitris Metaxas¹, Leon Axel⁴

¹ CBIM, Rutgers University, NJ. ² CSE Dept., Univ. of Texas at Arlington.

³ Piedmont Heart Institute, GA, USA. ⁴ Radiology department, NYU, USA

ABSTRACT

In this paper, we propose methods to extract the motion of papillary muscles from high resolution CT images, and quantitatively characterize them by extracting spatio-temporal skeletons. This method first reconstructs and visualizes detailed models of papillary muscles using a two-stage coarse-to-fine registration. To describe the model's shape and motion effectively and efficiently, high level abstractions of the models, i.e., the skeletons, are extracted with spatial and temporal constraints. Several skeleton-based indices are proposed to analyze the changes of model shapes and motions during a heart cycle. The experimental results show the robustness and efficiency of spatio-temporal skeletons, and the proposed indices are capable to demonstrate the differences between healthy and hypertrophic papillary muscles.

Index Terms— Papillary muscle, spatial-temporal skeleton, modeling, visualization

1. INTRODUCTION

Heart disease is a major public health problem in most countries around the world. Therefore, it is critical to detect and diagnose such diseases in early stages. Non-invasive imaging methods, e.g., computed tomography (CT) and magnetic resonance imaging (MRI), are being used widely to assist disease diagnosis. Most existing diagnosis methods generally fall into two categories: global function based and regional function based. Global function based methods mainly focus on using high-level measurements (e.g., ejection fraction (EF), ventricular volume [10]) to evaluate the condition of the heart. However, these approaches may fail to discover local abnormalities, such as regional effects of left ventricular hypertrophy (LVH), or even severe aortic stenosis (AS) [11]. Regional function based methods try to detect heart disease from regional and local indices, such as the strain and wall thickness [3]. However, these methods are still unable to reveal and characterize the detailed interior structures and their properties, which could be beneficial for more specific characterization of the nature and severity of heart disease [7].

The growing capabilities of imaging methods (e.g., high resolution CT, MRI) provide a wealth of information on the detailed structure and function of the heart [6]. Previous have

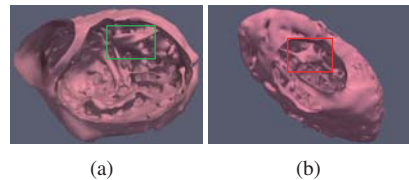


Fig. 1. Model meshes reconstructed from high resolution CT data of left ventricle (valves removed for better visualization). (a) Healthy heart. (b) Hypertrophic heart. These results capture many details inside the heart. The papillary muscles are marked with bounding boxes.

works mainly focused on automatic and global segmentation, without analyzing the potential of acquired detail information of individual main anatomical structures, such as the papillary muscle and the trabeculae. Nevertheless, these structures play very important roles in heart function, and they could be closely related to heart disease, such as, left ventricular hypertrophy [7, 9]. Papillary muscles, in particular, which connect the heart wall and the valves, control the correct blood flow by their contractions and relaxations. Therefore, it is potentially significant to visualize them and analyze their function during a heart cycle. In this paper, we propose a framework for reconstructing and visualizing the papillary muscle with its detailed structures from high resolution CT images, and extract the associated spatio-temporal skeletons for further shape and motion analysis. A two-stage coarse-to-fine registration method is employed to reconstruct the 3D+time models of papillary muscles. A skeleton is a geometric and topological abstraction of a 3D object, and has been shown to be effective in shape and motion analysis [1]. A spatio-temporal skeleton extraction and registration method is proposed to extract the skeletons and skeleton-mesh mappings for reconstructed papillary muscle model meshes. Furthermore, we conduct extensive skeleton-based analysis on representative healthy and hypertrophic hearts.

2. METHODOLOGY

Our proposed framework consists of two main steps: 1) two-stage coarse-to-fine registration, which builds the 3D+time model meshes for papillary muscles from the high resolution CT image data, 2) spatio-temporal skeleton extraction for these meshes. To do this, we first extract the skeleton for the

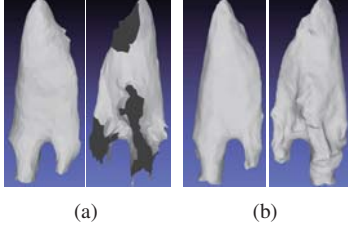


Fig. 2. The two-stage registration results of papillary muscle from the healthy heart. We show the frontal and back views of the first-stage (a) and the second-stage (b) registration results. (b) contains more details which are missing in (a).

base frame (i.e., the first acquired frame), build its skeleton-mesh mapping pattern, and then transfer the mapping pattern to other frames to obtain the desired skeletons.

Two-stage coarse-to-fine registration: We employ a deformable model based segmentation and registration algorithm [6] as the global stage. It generates 3D+time meshes from high resolution CT images with one-to-one vertex correspondences. Fig. 1 (a) and (b) show the segmentation results for a healthy heart and a hypertrophic heart, respectively.

Since the first-stage registration focuses on the global registration of the whole heart, it unavoidably brings in some reconstruction biases and noise for the local area of the papillary muscle (Fig. 2). Thus, we need to employ a finer second-stage registration on the papillary muscle area only. We manually select the papillary muscle from the global registered 3D model of the heart on the base frame, as shown in Fig. 2(a). The corresponding papillary muscle parts in the rest of the frames can be cropped out automatically, according to the one-to-one vertex correspondences. An adaptive-Focus Deformable Model (AFDM) [8] is then employed as the *second-stage* local registration, and more accurate and finer models of papillary muscles are obtained. The one-to-one vertex correspondences are also computed (Fig. 2(b)).

Spatio-temporal skeleton extraction: A skeleton is a low dimensional shape abstraction of an object mesh, so it has many advantages to represent the high level shape and motion [1]. To analyze the object shape at the skeleton level, we propose a spatio-temporal skeleton extraction algorithm to obtain the skeletons for all frames in a heart cycle, whose skeleton-mesh mappings are consistent spatially and temporally. Most existing skeleton extraction methods [1, 14, 13] mainly focus on how to extract the skeleton for a single object. If the skeletons of the papillary muscle meshes are extracted individually without considering the spatial and temporal constraints, the results may not be stable and consistent. They may also have different number of nodes and different skeleton-mesh mapping patterns. Moreover, the computational cost for a single skeleton extraction method is high, and it is time-consuming to run it for every frame. Therefore, extracting spatio-temporal skeletons efficiently is essential for further shape and motion analysis. Our spatio-temporal skeleton extraction algorithm includes three steps: a) single skeleton extraction, b) skeleton mesh mapping, and c) skeleton reg-

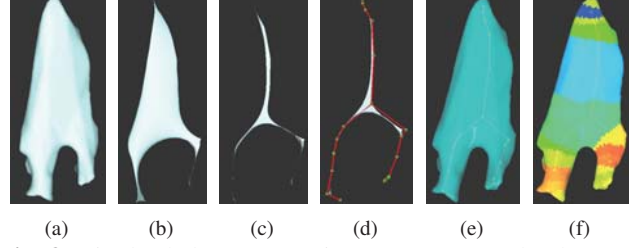


Fig. 3. Single skeleton extraction. (a) Input mesh. (b) Intermediate results after a few volume contractions. (c) Approximate zero-volume mesh after contractions. (d) Extracted 1D curve-skeleton. (e) Extracted skeleton visualization with input mesh. (f) The skeleton-mesh mapping result. Each color of mesh surface corresponds to one skeleton node separately.

istration, which are introduced below.

a) *Single skeleton extraction:* In order to generate a 1D curve skeleton, which abstracts the given object topologically, we first make the object contract until it turns into an approximate zero-volume mesh by iteratively smoothing, and then convert the zero-volume mesh into a 1D curve skeleton.

Given a mesh $G = (V, E, F)$, with vertices V , edges E , and faces F , where $V = [v_1^T, \dots, v_n^T]^T$ are the vertex positions. The volume reduction process is based on geometry contractions that iteratively smooth and collapse the mesh without ruining the topological structure. This contraction is formulated as an energy minimization problem involving two terms: a *contraction term* based on the discrete Laplace operator that removes the geometry details along the approximate normal directions, and an *attraction term* that uses the mesh vertices as anchors to retain necessary topological structure in the collapsing shape [1]. The conjugate normal direction for the contraction is defined as L , the $n \times n$ curvature-flow Laplace operator with elements:

$$L_{ij} = \begin{cases} w_{ij} = \cot(\alpha_{ij}) + \cot(\beta_{ij}), & \text{if } (i, j) \in E \\ \sum_{(i,k) \in E}^k (-w_{ik}), & \text{if } i = j \\ 0, & \text{otherwise} \end{cases} \quad (1)$$

where α_{ij} and β_{ij} are the opposite angles corresponding to the edge (i, j) [5].

The new vertex position V' of the contraction result for V can be obtained by solving the discrete Laplace equation: $LV' = 0$. This equation is also called *contraction constraints*, which tries to remove the normal details and contract the mesh geometry. To ensure the contracted mesh abstracts the original shape well, all the vertices are constrained to keep their current positions as soft constraints. The constraint can be denoted as $V' = V$.

We put these two constraints in a single Laplacian system:

$$\begin{bmatrix} W_L L \\ W_H V \end{bmatrix} V' = \begin{bmatrix} 0 \\ W_H V \end{bmatrix} \quad (2)$$

where W_L, W_H are the weights to balance the *contraction* and *attraction* constraints in the contraction iterations [1]. After contracting the object step by step until it becomes an approximate zero-volume mesh (Fig. 3(c)), a series of edge-collapses [1] is employed to remove collapsed faces from the

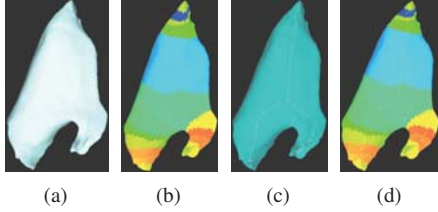


Fig. 4. The procedure of skeleton registration. (a) An input mesh for skeleton extraction. (b) Skeleton-mesh mapping transferred from base frame. Skeleton result visualization with input mesh (c) and skeleton-mesh mapping (d).

degenerated mesh, until all faces have been removed. One example of a extracted skeleton can be found in Fig. 3(d).

b) Skeleton mesh mapping. After the skeleton is extracted from the mesh, we need to find the mapping pattern between the skeleton nodes and the faces of the mesh. The mapping results can reveal the physical meanings of the skeleton abstraction. It is also a key prerequisite for the following skeleton registration. Suppose the extracted skeleton of mesh $G = (V, E, F)$ is $S = (SV, SE)$ with skeleton nodes SV and edges SE . The mapping is between the faces $F = \{f_1, f_2, \dots, f_m\}$ and the skeleton nodes $SV = \{SV_1, SV_2, \dots, SV_k\}$. The union of all the faces mapping to the same node is called a *component*. $GeoDist(f_i, SV_j)$, the *geodesic distance* between a face f_i and a skeleton node SV_j , is defined as the average Euclidean distance between all the vertices of face f_i and node SV_j . Intuitively, faces should be mapped to the skeleton nodes with the shortest geodesic distance. However, the boundaries between different components should have deep concavities rather than flat surface transitions. Therefore, it is not enough to only consider the geodesic distance. The curvature of the mesh surface is also a good indicator for the boundaries of the different components. We define the *angular distance* between two faces f_p and f_q as :

$$AngDist(f_p, f_q) = (1 - \cos\alpha_{pq}). \quad (3)$$

where α_{pq} is the angle between the normal vectors of f_p and f_q . The angular distance between a face f_p with a skeleton nodes SV_j (denoted as $AngDist(f_p, VS_j)$), is the shortest distance between f_p and all the faces already mapped to SV_j . So the index of skeleton node associated with face f_p is:

$$arg\min\{GeoDist(f_p, SV_d) + \mu AngDist(f_p, VS_d)\} \quad (4)$$

where $d \in [1, \dots, k]$, μ is the weight used to balance between geodesic and angular distance. $\mu = 2$ in our setting.

The initial faces mapped to the skeleton nodes are selected by only considering the geodesic distance. Other faces are then mapped to the skeleton one by one according to Eq. 4. An example result is shown in Fig. 3(f), and the component segmentations are promising, e.g., two branch muscles are segmented out properly.

c) Skeleton registration. Since the one-to-one vertex correspondences among all the papillary muscle meshes have been built using a two-stage coarse-to-fine registration, the

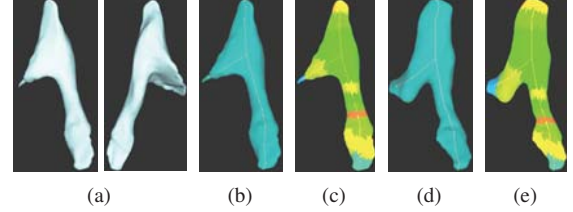


Fig. 5. Results of the hypertrophic papillary muscle. (a) Reconstruction result (front & back views). (b) Extracted skeleton result. (c) Skeleton-mapping result. (d, e) spatio-temporal skeleton extraction results on another hypertrophic frame.

mesh component segmentations can be easily transferred from one mesh to another one. Take Fig. 4(a) as a new input mesh to illustrate our method. Fig. 4(b) shows one mapping result transferred from Fig. 3(f). Skeleton nodes are the abstractions of the corresponding components, so their locations can be referred from these components. The location of a skeleton node is calculated using the weighted average of all the coordinates of the vertices belonging to the corresponding component. The weights are inversely proportional to the corresponding node-vertex distances of the base frame. The skeleton result for this example is shown in Figs. 4(c) and 4(d). In this way, the skeletons of other meshes can also be obtained. Our method only has to run the single skeleton extraction algorithm once for the base frame. Thus, it is much more efficient than extracting the skeleton for each frame.

3. EXPERIMENTS

Data Description: We collected CT scans from healthy and hypertrophic hearts. The CT images were obtained from a 320-MSCT scanner (Toshiba Aquilion ONE). A whole heart can be captured in a single rotation using this advanced dynamic volume CT scanner, and a high isotropic volumetric resolution ($0.3mm$) can be achieved. A conventional ECG-gated contrast-enhanced CT angiography protocol is adopted to acquire the CT image data. For each cardiac cycle, 10 cardiac 3D+time CT images were acquired, which are equally distributed in a single cycle of cardiac contraction. The resolution of each time frame is 512 by 512 by 320 pixels. The reconstructed models for the hearts can be found in Fig. 1.

Visualization: The visualizations for the papillary muscle of the healthy heart are shown in Fig. 2. The results of single skeleton extraction, skeleton-mesh mapping, and skeleton registration are shown in Fig. 3. Fig. 5 shows the results of two frames of the hypertrophic heart. The branching structures, which attach the papillary muscle to the myocardium, are also visualized clearly in these figures. This shows that the papillary muscles are separate structures rather than solid portions of the heart wall, as was the conventional belief [2]. Apparently, the papillary muscles from the healthy heart and the hypertrophic heart are quite different in appearance. More quantitative analysis on the differences between healthy and hypertrophic papillary muscles will be conducted.

Quantitative results: In order to further explore the function of papillary muscles and the differences between

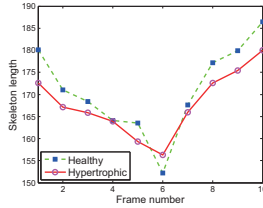


Fig. 6. Skeleton length comparison of healthy and hypertrophic papillary muscles. Larger changing range indicates more intense contraction and stretch.

healthy and hypertrophic hearts, we performed some quantitative analysis based on the reconstruction results and the extracted spatio-temporal skeletons. We also propose several new indices to measure the cardiac function.

Volume index. Volume is a global descriptor, which indicates some cardiac disabilities. Since the volume of papillary muscle won't change much during a heart cycle, we compare the average volumes of the papillary muscles. The average volume of the healthy papillary muscles is 2825 mm^3 , while the average volume of the hypertrophic papillary muscles is 4677 mm^3 . This result shows that the volume of hypertrophic papillary muscles is much bigger than the healthy ones.

Skeleton length index. The stretch of a papillary muscle can be mainly measured by the length of its skeleton, which is the sum of all the edges of the skeleton. The length is measured in voxels, so it won't suffer from scale issues. Fig. 6 shows the skeleton length changes of healthy and hypertrophic papillary muscles in a heart cycle. The reduction of skeleton length indicates the muscle contraction, while the increase means relaxation. One contraction and one relaxation are captured for both healthy and hypertrophic papillary muscles in one heart cycle. The value range of healthy papillary muscles are larger, which indicates the contractions of the healthy ones are more intense, and thus more functional.

Skeleton Motion index. Cardiac motion is an important indicator of heart health [4, 12], and the deformation of papillary muscles plays an important roles. We calculated the skeleton motion for healthy and hypertrophic papillary muscles to explore their differences. To validate that the skeletons are good abstractions of the meshes, the mesh motions are also computed for reference. Skeleton motion and mesh motion are defined to be the average location displacements of skeleton nodes and mesh vertices, respectively (measured in voxels). Fig. 7 shows that the range of the skeleton motions of healthy papillary muscles is much larger than hypertrophic ones, which means the healthy papillary muscles have better functional behaviors, e.g., quick deformations, thorough relaxations. The motions of skeletons and meshes are also compared, and there are little differences between them regardless of different conditions of papillary muscles. Thus the skeleton is a promising way to abstract mesh, besides its many rewarding benefits in efficiency and robustness.

4. CONCLUSIONS

In this paper, we proposed a method to reconstruct and visualize dynamic papillary muscles from high resolution CT im-

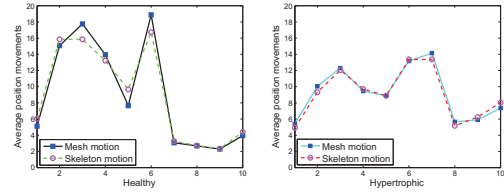


Fig. 7. Results of the mesh and skeleton motion for the healthy (left) and hypertrophic (right) papillary muscles in a heart cycle. Each figure compares the motion between the meshes and their high-level abstractions (i.e., skeletons).

ages. The reconstructed models contain substantial and unprecedented details. Furthermore, a novel mesh abstraction approach, spatio-temporal skeleton extraction method, is proposed to extract skeletons from sequence frames and analyze papillary muscle functions during a heart cycle. Extensive experiments on skeleton-based indices show the capabilities of our method to capture the differences between healthy and hypertrophic hearts, and its robustness and efficiency.

This work is supported by the Multiscale Quantification of 3D LV Geometry from CT project, sponsored by NHLBI under Grant Award Number 5R21HL088354-02.

5. REFERENCES

- [1] O. K. Au, C. Tai, H. Chu, D. Cohen-Or, and T. Lee. Skeleton extraction by mesh contraction. *Siggraph*, 2008.
- [2] L. Axel. Papillary muscles do not attach directly to the solid heart wall. *Circulation*, 2004.
- [3] E. Castillo, A. C. Lima, and D. A. Bluemke. Regional myocardial function: Advances in MR imaging and analysis. *Radiographics*, 2003.
- [4] H. Delingette and et.al. Personalization of cardiac motion and contractility from images using variational data assimilation. *TBE*, 2011.
- [5] M. Desbrun, M. Meyer, P. Schroder, and A. H. Barr. Implicit fairing of irregular meshes using diffusion and curvature flow. *Siggraph*, 1999.
- [6] M. Gao and et.al. 4D cardiac reconstruction using high resolution CT images. *FIMH*, 2011.
- [7] M. Janik and et.al. Effects of papillary muscles and trabeculae on left ventricular quantification: increased impact of methodological variability in patients with left ventricular hypertrophy. *Journal of Hypertension*, 2008.
- [8] D. Shen and C. Davatzikos. An adaptive-focus deformable model using statistical and geometric information. *TPAMI*.
- [9] L. Spreeuwiers, S. Bangma, R. Meerwaldt, E. Vonken, and M. Breeuwer. Detection of trabeculae and papillary muscles in cardiac MR images. *Computers in Cardiology*, 2005.
- [10] D. Ye and et.al. Morphological classification: Application to cardiac MRI of tetralogy of fallot. *FIMH*, 2011.
- [11] A. A. Young. Assessment of cardiac performance with magnetic resonance imaging. *Current Cardiol. Rev.*, 2006.
- [12] D. P. Zhang and et.al. Coronary artery motion modeling from 3D cardiac CT sequences using template matching and graph search. *ISBI*, 2010.
- [13] S. Zhang, J. Huang, and D. N. Metaxas. Robust mesh editing using laplacian coordinates. *Graphical Models*, 2011.
- [14] W. Zhou, H. Li, and X. Zhou. 3D dendrite reconstruction and spline identification. *MICCAI*, 2008.